Monolayer 1T-LaN_2 : Dirac spin-gapless semiconductor of p-state and Chern insulator with a high Chern number

Monolayer 1T-LaN_2: Dirac spin-gapless semiconductor of *p*-state and Chern insulator with a high Chern number

Linyang Li,[1,2] Xiangru Kong,[3,a)] Xin Chen,[4,b)] Jia Li,[1] Biplab Sanyal,[4] and François M. Peeters,[5,2]

[1]*School of Science, Hebei University of Technology, Tianjin 300401, China*

[2]*Department of Physics, University of Antwerp, Groenenborgerlaan 171, B-2020 Antwerp, Belgium*

[3]*Center for Nanophase Materials Sciences, Oak Ridge National Laboratory, Oak Ridge, Tennessee 37831, USA*

[4]*Department of Physics and Astronomy, Uppsala University, SE-75120 Uppsala, Sweden*

[5]*Department of Physics and Astronomy, Key Laboratory of Quantum Information of Yunnan Province, Yunnan University, Kunming 650091, China*

Abstract

Two-dimensional transition-metal dinitrides have attracted considerable attention in recent years due to these rich magnetic properties. Here, we focus on the rare-earth-metal elements and propose a monolayer of lanthanum dinitride with a 1T structural phase, 1T-LaN_2. Using first-principles calculations, we systematically investigated the structure, stability, magnetism, and band structure of this material. It is a flexible and stable monolayer exhibiting a low lattice thermal conductivity, which is promising for future thermoelectric devices. The monolayer shows ferromagnetic ground state with a spin-polarized band structure. Two linear spin-polarized bands cross at the Fermi level forming a Dirac point, which is formed by the *p* atomic orbitals of the N atoms, indicating that monolayer 1T-LaN_2 is a Dirac spin-gapless semiconductor of *p*-state. When the spin-orbit coupling is taken into account, a large nontrivial indirect

band gap (86/354 meV) can be opened at the Dirac point, and three chiral edge states are obtained, corresponding to a high Chern number of $C = 3$, implying that monolayer 1T-LaN_2 is a Chern insulator. Importantly, this kind of band structures is expected to occur in more monolayers of rare-earth-metal dinitride with a 1T structural phase.

[a)]Author to whom correspondence should be addressed: kongx@ornl.gov (Xiangru Kong)

[b)]Author to whom correspondence should be addressed: xin.chen@physics.uu.se (Xin Chen)

Two-dimensional (2D) materials can exhibit extraordinary physical and chemical properties, offering distinct features for the next-generation of nanoscale devices. Among those materials, monolayer MoS_2 was realized in 2005 by micromechanical exfoliation,[1] and demonstrated to be a promising material for atomic-thick transistors, which was the start of an interesting class of 2D transition-metal dichalcogenides. The typical crystal structure of MoS_2 is 1H, which exhibits a semiconductor band structure with a direct band gap and valley polarization property at the K and K' points.[2] Besides the 1H structural phase, the 1T and 1T' structural phases were also proposed. However, 1T-MoS_2 is thermodynamically unstable, which is the main drawback impeding its practical application, although it exhibits superior hydrogen evolution reaction over 1H-MoS_2, as was recently confirmed experimentally.[3] The monolayer 1T'-MoS_2 was predicted to be a quantum spin Hall (QSH) insulator.[4] Many interesting physical and chemical properties were observed in these monolayers of MoS_2, except magnetism. A natural idea is to change the Mo/S element by other elements. In 2015, Wang *et al.* successfully synthesized 3R-MoN_2 by a high-pressure route,[5] which is a layered structure similar to 1H-MoS_2. Then, monolayer 1H-MoN_2 was theoretically predicted to exhibit two structural phases (α and β),

corresponding to ferromagnetic (FM) and antiferromagnetic (AFM) states, respectively.[6] ReN_2 crystal, which shows a similar structure with MoN_2, can be exfoliated into thin films as demonstrated in a recent experiment.[7] These studies opened a door to study magnetic states in N-based materials.[8-10] Further studies showed that the 1T structural phase could be stable beside the 1H structural phase.[11,12] Consequently, an emerging class of 2D materials, transition-metal dinitrides with the 1H/1T structural phase were proposed, where rich magnetic states can be found.

Chern insulators are another important set of 2D materials because they can realize the quantum anomalous Hall (QAH) effect,[13] which therefore are also called QAH insulators. Compared to the QSH effect, the realization of the QAH effect requires more stringent conditions.[14-16] Recently, the operating temperature to realize the QAH effect has increased to 1.4 K in $MnBi_2Te_4$ thin flake with an intrinsic FM state,[17] much higher than that (< 100 mK) of the chromium-doped $(Bi,Sb)_2Te_3$ where the FM state is introduced by Cr-doping.[18] However, compared to the experimental operating temperature (100 K for 1T'-WTe_2 system) for the QSH effect,[19,20] 1.4 K is still very low. This temperature is mostly determined by the value of the nontrivial band gap arising from the spin-orbit coupling (SOC) effect. To achieve a large nontrivial band gap, many theoretical structures with an intrinsic FM state have been proposed, in particular, the 2D transition-metal trihalides.[21-29] However, these nontrivial band gaps are still not optimistic. Therefore, it is of crucial importance to search for QAH insulators with an intrinsic FM state and a larger nontrivial gap.

Based on the 1T/1H structural phase, Liu *et al.* performed a structural search for 2D transition-metal dinitrides by using most common transition-metal elements (Ti-Fe, Zr-Ru, Hf-Os, Y).[11,12] From the point of view of the band structure, most of these monolayers show a spin-polarized metal band structure. However, only monolayer 1T-YN_2 is very special and exhibits a spin-polarized Dirac band structure

without SOC[12] and a Chern insulator state with SOC.[14] We should notice that the Y element is not only a transition-metal element but also a rare-earth-metal element. Considering the chemical similarity of the rare-earth-metal elements, more monolayers of rare-earth-metal dinitrides should be interesting. Therefore, using the 1T structural phase, we propose a monolayer of lanthanum dinitride, 1T-LaN_2, which is a very interesting stable 2D magnetic material. Using first-principles calculations, we investigated the structure, dynamical stability, magnetism, and band structure of monolayer 1T-LaN_2.

Our first-principles calculations were performed using the Vienna *ab initio* simulation package (VASP) code,[30-32] implementing density functional theory (DFT). The electron exchange-correlation functional was treated by using the generalized gradient approximation (GGA) in the form proposed by Perdew, Burke, and Ernzerhof (PBE).[33] The atomic positions and lattice vectors were fully optimized using the conjugate gradient (CG) scheme until the maximum force on each atom was less than 0.01 eV/Å. The energy cutoff of the plane-wave basis was set to 520 eV with an energy precision of 10^{-5} eV. The Brillouin zone (BZ) was sampled by using a 27×27×1 Γ-centered Monkhorst-Pack grid. The vacuum space was set to at least 20 Å in all the calculations to minimize artificial interactions between neighboring slabs. The phonon spectrum was calculated within the PHONOPY code.[34]

The investigated monolayer 1T-LaN_2 is displayed in Fig. 1(a). It has a hexagonal lattice with a 1T structural phase, where each La atom is bonded to six N atoms. The 1T structural phase has been not only realized in experiments, such as 1T-MoS_2,[3] 1T-TaS_2,[35] and 1T-$TiSe_2$,[36] but also widely applied for stable structural searches, such as transition-metal dihalides[37] and transition-metal dinitrides,[11] indicating its rationality. The optimized lattice constant, La-N bond length, and N-N distance along the *z*-direction are 4.05 Å, 2.47 Å, and 1.60 Å, respectively. Notice that the lattice constant and bond length, 4.05/2.47 Å is slightly larger than the 3.76/2.34 Å of monolayer 1T-YN_2,[12] which is due to the larger atomic radius of

La. The mechanical property of monolayer 1T-LaN_2 was further investigated in Part I of the Supplementary Material.[38,39] The in-plane Young's modulus and Poisson's ratio in arbitrary directions are nearly isotropic, as shown in Fig. S1. The Young's modulus is about 39 N/m, much smaller than 124.24 N/m of monolayer MoS_2 (1H),[40] showing that the monolayer is more flexible. The Poisson's ratio is about 0.55 in arbitrary directions, where the difference between the maximum and minimum of the ratios is smaller than 2%, implying isotropic elasticity.

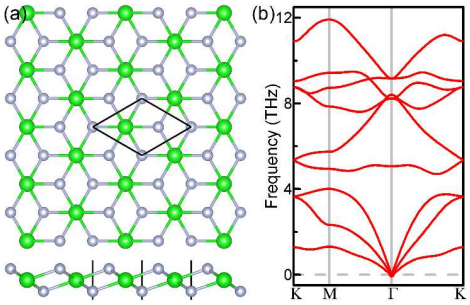

Fig. 1. Schematic representations (top and side views) of monolayer 1T-LaN_2 (a) and its phonon spectrum along the high-symmetry path of the first BZ (b). The green dots are La atoms, and the silver dots are N atoms. The black box is the unit cell.

The cohesive energy is obtained from the expression $E_{coh} = (E_{La}+2E_N-E_{LaN2})/3$, where E_{La}/E_N is the total energy of a single La/N atom, and E_{LaN2} is the total energy per unit cell of monolayer 1T-LaN_2.[41] The calculated cohesive energy is 4.32 eV/atom, which is slightly larger than 4.28 eV/atom of monolayer 1T-YN_2,[12] indicating its experimental feasibility. To further assess the stability of monolayer 1T-LaN_2, we studied its lattice dynamics by calculating the phonon spectrum, which is shown in Fig. 1(b). It is free from imaginary frequency modes, which indicates that monolayer 1T-LaN_2 is dynamically stable. In view

of the low cutoff frequency of acoustic and optical phonons, the 1T-LaN_2 structure is expected to have a low lattice thermal conductivity.[42] The calculation details of its lattice thermal conductivity is in Part II of the Supplementary Material.[43-47] The lattice thermal conductivity of monolayer 1T-LaN_2 at room temperature is κ_L = 13.9 W/mK (Iterative, Fig. S2), which is lower than 34.5±4 W/mK of monolayer MoS_2 (1H)[48] and comparable to 11.6 W/mK of stanene.[49] The low lattice thermal conductivity makes monolayer 1T-LaN_2 a promising material for thermoelectric devices.

We then investigated the magnetic ground state, the origin of the magnetic moment,[12,50,51] and the Curie temperature[25,52,53] for monolayer 1T-LaN_2 in Part III of the Supplementary Material. Based on the FM ground state with the magnetic moment of $3\mu_B$, the electronic band structures of monolayer 1T-LaN_2 obtained from PBE calculations are shown in Fig. 2. Considering the band structure without SOC, we found that the degeneracy of the two spin channels is removed, resulting in a spontaneous spin-polarized band structure (spin-up bands are in blue and spin-down bands are in red), as shown in Fig. 2(a). Notice that there is a large spin-splitting of the two kinds of bands. Considering the valence bands of spin-up (blue lines), all of them are below the Fermi level, while three spin-down bands (red lines) are above the Fermi level, corresponding to the magnetic moment of $3\mu_B$. Considering the occupied states below the Fermi level, the spin-up states are much more populated than the spin-down states, leading to the spin-polarized electron density of spin-up, as shown in Fig. S3(a) (blue area around the N atoms). For the spin-down bands, the valence and conduction bands meet at a single point at the Fermi level, giving rise to a Dirac point located at the D point along the K-M line of the first BZ, as shown in Fig. 2(a). Each of the two bands forming the Dirac point is linear with a Fermi velocity of $4.3\times10^5/1.3\times10^5$ m/s, which is comparable to 3.74×10^5 m/s of monolayer 1T-YN_2.[12] To fully confirm the existence of the linear Dirac point, we used the more sophisticated Heyd-Scuseria-Ernzerhof (HSE06)[54,55] hybrid functional method

to calculate the band structure without SOC, which is shown in Fig. S4(a). The spin-polarized band structure, including spin-up/spin-down bands (blue/red) and a Dirac point at the Fermi level, can be clearly seen. The Dirac point is formed by two spin-down bands and located at the D' points along the K-M line of the first BZ. Each of the two bands forming the Dirac point is linear with a Fermi velocity of $4.5\times10^5/2.9\times10^5$ m/s. The fact that the PBE and HSE06 methods both give a similar band structure close to the Fermi level, including the Dirac point, strengthens our belief in the validity of the band structure around the Fermi level. Remarkably, this spin-polarized band structure without SOC including a linear Dirac point at the Fermi level indicates that monolayer 1T-LaN_2 should be a Dirac spin-gapless semiconductor (DSGS),[56-60] which was proposed by X. L. Wang in 2008.[56]

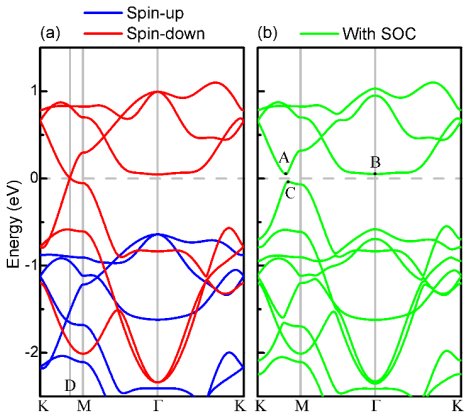

Fig. 2. Band structures without SOC (a) and with SOC (b) of monolayer 1T-LaN_2 from PBE calculations.

DSGSs can be further classified into *p*-state or *d*-state type depending on the degree of contribution of either the *p* or *d* atomic orbitals to the Dirac state.[58-60] To investigate the origin of the Dirac point at the Fermi level, we calculated the projected density of states (PDOS) in Fig. 3. First, let us focus on the

PDOS analysis of the different atoms. It is clear that the main states around the Fermi level come from the N atoms while the contributions of the La atoms are very small, as shown in Fig. 3(a). After the main contributions of the N atoms are confirmed, we further analyzed the contributions of the different atomic orbitals of the N atoms. From Fig. 3(b), it is clear that the *s* atomic orbital around the Fermi level contributes much less than the $p_x/p_y/p_z$ atomic orbital. Based on the PDOS analysis, the band structure close to the Fermi level, including the Dirac point, is mainly built up by the *p* (p_x, p_y, and p_z) atomic orbitals of the N atoms, and therefore monolayer 1T-LaN_2 should be a DSGS of *p*-state. To date, the majority of DSGS members are *d*-state type materials.[58] Monolayer 1T-LaN_2 can enrich the family of *p*-state DSGSs, and may become a promising 2D material for application in spintronic devices.

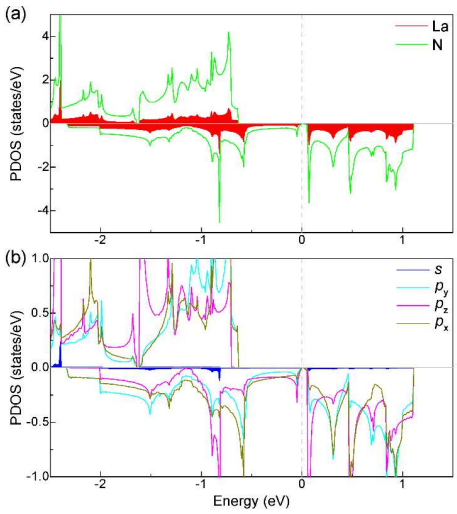

Fig. 3. PDOS of the La and N atoms (a) and PDOS of the *s* and $p_x/p_y/p_z$ atomic orbitals (N atoms) (b) for monolayer 1T-LaN_2. The results are from the calculations of PBE without SOC.

SOC is a relativistic effect and is very important for systems containing heavy atoms. Since there are La atoms in our monolayer, we should take the SOC effect into account in the calculations of the band structure. The electronic band structure of monolayer 1T-LaN_2 obtained from PBE+SOC calculations is shown in Fig. 2(b). An indirect band gap (E(CA) = 86 meV) is opened at the linear Dirac point. The valence band maximum is found at the C point. However, we should notice that there are two conduction band minimums, the A and B points. Since the A and B (at the Γ point of the first BZ) points have almost the same energy level ($|E(A)-E(B)| < 1$ meV), the global indirect band gap is E(CA) = E(CB) = 86 meV. Using HSE06+SOC (Fig. S4(b)), an enhanced indirect band gap (E(C'A') = 354 meV) is also opened at the linear Dirac point, which is much larger than E(CA) = 86 meV obtained from PBE+SOC calculations. Since the energy level of B' point (at the Γ point of the first BZ) is much higher than that of the A' point (E(B') > E(A')), the global indirect band gap is E(C'A') = 354 meV for the HSE06 band structure with SOC. Monolayer 1T-YN_2 has a SOC gap of 29.7 meV at the PBE level and 97.5 meV at the HSE06 level,[14] which are much smaller than the SOC gap of 86 meV at the PBE level and 354 meV at the HSE06 level for monolayer 1T-LaN_2. Although the Dirac point is mainly formed by the *p* atomic orbitals of the N atoms in the monolayer 1T-LaN_2/1T-YN_2[12,14] while the contributions of the La/Y atoms for the Dirac point are very small, the SOC effect of La atom is more pronounced than that of Y atom, which can lead to a larger SOC coefficient, resulting in a larger SOC gap. Generally speaking, for the band structure with a band gap, the PBE method typically underestimates the band gap while the result of the HSE06 method is larger and more accurate than the value obtained from the PBE method, which has been confirmed in many systems. Despite the difference in the value of the SOC band gap, the main characters that include the position of Dirac point at the first BZ without SOC and the band gap opening at the Dirac point with SOC are qualitatively the same. In the following calculations, we will

consider the band structures at the PBE level.

Opening a SOC band gap at the Dirac point is a key sign of topological property. Since the bands close to the Fermi level, including the Dirac point, are mainly formed by the p_x, p_y, and p_z atomic orbitals of the N atoms (Fig. 3), an effective tight-binding Hamiltonian was constructed by the p_x, p_y, and p_z atomic orbitals of the N atoms. A further study on the topological property was carried out within the WannierTools package.[61,62] To identify the topological property of the gapped state of monolayer 1T-LaN_2, we calculated its chiral edge states, as shown in Fig. 4(a). With the effective concept of principle layers, an iterative procedure to calculate the Green's function for a semi-infinite system was employed.[63] Three chiral edge states connecting the valence and conduction band areas emerge inside the bulk gap of a semi-infinite system, indicating that the band gap of 86 meV is nontrivial, which is large enough to realize the QAH effect at room temperature. On the other hand, according to the bulk-edge correspondence, three chiral edge states indicate a high Chern number (C) in a time-reversal symmetry broken system. To demonstrate this, we used the Wilson loop method to keep track of the hybrid Wannier charge centers (WCCs) along one primitive reciprocal lattice vector k_y:

$$\bar{x}_n(k_y) = \frac{i}{2\pi}\int_{-\pi}^{\pi} dk_x \langle u_n(k_x, k_y)|\partial k_x|u_n(k_x, k_y)\rangle,$$

where $u_n(k_x, k_y)$ is the periodic part of the Bloch function $\psi_n(k_x, k_y)$. Chern number C is defined as the change of the sum of hybrid WCCs $\bar{x}_n$ during a continuous deformation:

$$C = \sum_n \bar{x}_n(2\pi) - \sum_n \bar{x}_n(0).$$

As can be seen from Fig. 4(b), the sum of hybrid WCCs shifts upwards with the winding number 3, giving rise to the Chern number $C = 3$, which is the same result for monolayer 1T-YN_2.[14] The high Chern number of $C = 3$ corresponds to the three chiral edge states, which can provide strong currents and signals when applied in electronic devices. In a recent experiment, a high Chern number of $C = 2$ can be realized

in the 9- and 10-layer $MnBi_2Te_4$.[64] In theory, the Chern number of most 2D Chern insulators is $|C| = 1$,[22-29,53] while the Chern insulators with a Chern number of $|C| \geq 2$ have been very scarce.[14,21,65-68] Although using additional chemical means, such as the adsorption of transition-metal atoms on graphyne, can realize a Chern number of $C = -3$,[69] it is not an intrinsic property of the material, which increases the difficulty of its experimental realization. The proposed monolayer 1T-LaN_2 should be a good candidate material for Chern/QAH insulator due to the large nontrivial band gap and the high Chern number of $C = 3$.

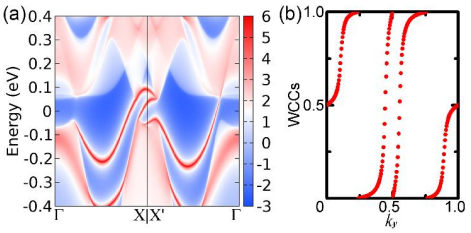

Fig. 4. The chiral edge states of a semi-infinite plane $(\bar{1}10)$ (a) and the evolution of the sum of the hybrid WCCs (b) for monolayer 1T-LaN_2.

So far, we have confirmed the similarity in band structure between monolayer 1T-LaN_2 and monolayer 1T-YN_2.[12,14] However, the La and Y elements are only 2 of the 17 rare-earth-metal elements. A natural question arises: Can this kind of band structures occur in more rare-earth-metal dinitrides with the 1T structural phase? To confirm it, we tried another rare-earth-metal element Lu, and we calculated the band structures of monolayer 1T-LuN_2 in the FM state (magnetic moment of $3\mu_B$), as shown in Fig. S5. Without SOC, the spin-polarized band structure can be clearly seen, and a Dirac point is found at the Fermi level along the K-M line of the first BZ, which is formed by two linear bands (spin-down) with a

Fermi velocity of $4.6\times10^5/4.0\times10^5$ m/s, indicating it is a DSGS. When including SOC, a SOC band gap (80 meV) is opened at the Dirac point. The band gap of 80 meV is nontrivial, which is confirmed by the three chiral edge states connecting the valence and conduction band areas with the Chern number $C = 3$, as shown in Fig. S6, similar to the results of monolayer 1T-LaN_2. Based on the band structures without and with SOC of monolayer 1T-YN_2[12,14]/1T-LaN_2/1T-LuN_2, three monolayers of rare-earth-metal dinitride with 1T structural phase can exhibit a special nontrivial band structure that allows achieving QAH effect and therefore, it would be interesting to investigate other rare-earth-metal elements. More 2D Chern insulators are expected to be found in monolayers of rare-earth-metal dinitride.

In summary, using first-principles calculations, we predict a monolayer of rare-earth-metal dinitride, 1T-LaN_2, to be a DSGS of *p*-state and a Chern insulator with a high Chern number ($C = 3$) and a large nontrivial indirect band gap of 86 meV (PBE+SOC), which increases to 354 meV when we used HSE06+SOC. The monolayer is in the 1T structural phase, and its dynamical stability is confirmed by the phonon spectrum, which is free from imaginary frequency modes. We predict that the magnetic ground state is FM state with magnetic moment of $3\mu_B$, corresponding to a spin-polarized band structure. Monolayer 1T-LaN_2 is a *p*-state DSGS without SOC, while it becomes a Chern insulator with SOC. This kind of band structures is expected to occur in more monolayers of rare-earth-metal dinitride with a 1T structural phase. As an example, we confirmed this in monolayer 1T-LuN_2. The large nontrivial band gap and the high Chern number of monolayer 1T-LaN_2/1T-LuN_2 are beneficial for achieving the QAH effect at room temperature.

See the Supplementary Material for mechanical property (Part I), lattice thermal conductivity (Part II), magnetic property (Part III), HSE06 band structures of monolayer 1T-LaN_2 (Part IV), and band

structures of monolayer 1T-LuN_2 and its topological property (Part V).

DATA AVAILABILITY

The data that support the findings of this study are available from the corresponding author upon reasonable request.

This work was supported by the Natural Science Foundation of Hebei Province (Grant No. A2020202031), the FLAG-ERA project TRANS2DTMD, the Swedish Research Council project grant (2016–05366), and the Swedish Research Links program grant (2017–05447). The resources and services used in this work were provided by the VSC (Flemish Supercomputer Center), funded by the Research Foundation - Flanders (FWO) and the Flemish Government, and Swedish National Infrastructure for Computing (SNIC). A portion of this research (Xiangru Kong) was conducted at the Center for Nanophase Materials Sciences, which is a DOE Office of Science User Facility. Xin Chen thanks the China scholarship council for financial support from the China Scholarship Council (CSC, No. 201606220031).

REFERENCES

[1]K. S. Novoselov, D. Jiang, F. Schedin, T. J. Booth, V. V. Khotkevich, S. V. Morozov, and A. K. Geim, PNAS **102**, 10451 (2005).

[2]S. Manzeli, D. Ovchinnikov, D. Pasquier, O. V. Yazyev, and A. Kis, Nat. Rev. Mater. **2**, 17033 (2017).

[3]K. Zhang, B. Jin, Y. Gao, S. Zhang, H. Shin, H. Zeng, and J. H. Park, Small **15**, 1804903 (2019).

[4]X. Qian, J. Liu, L. Fu, and J. Li, Science **346**, 1344 (2014).

[5]S. Wang, H. Ge, S. Sun, J. Zhang, F. Liu, X. Wen, X. Yu, L. Wang, Y. Zhang, H. Xu, J. C. Neuefeind, Z. Qin, C. Chen, C. Jin, Y. Li, D. He, and Y. Zhao, J. Am. Chem. Soc. **137**, 4815 (2015).

[6]Y. Wang, S.-S. Wang, Y. Lu, J. Jiang, and S. A. Yang, Nano Lett. **16**, 4576 (2016).

[7]M. Onodera, F. Kawamura, N. T. Cuong, K. Watanabe, R. Moriya, S. Masubuchi, T. Taniguchi, S. Okada, and T. Machida, APL Mater. **7**, 101103 (2019).

[8]W. Li, C. Guo, X. Xin, X. Shi, and Y. Zhao, Appl. Surf. Sci. **487**, 519 (2019).

[9]X. Zhang, Z. Yu, S.-S. Wang, S. Guan, H. Y. Yang, Y. Yao, and S. A. Yang, J. Mater. Chem. A **4**, 15224 (2016).

[10]F. Wu, C. Huang, H. Wu, C. Lee, K. Deng, E. Kan, and P. Jena, Nano Lett. **15**, 8277 (2015).

[11]J. Liu, Z. Liu, T. Song, and X. Cui, J. Mater. Chem. C **5**, 727 (2017).

[12]Z. Liu, J. Liu, and J. Zhao, Nano Res. **10**, 1972 (2017).

[13]F. D. M. Haldane, Phys. Rev. Lett. **61**, 2015 (1988).

[14]X. Kong, L. Li, O. Leenaerts, W. Wang, X.-J. Liu, and F. M. Peeters, Nanoscale **10**, 8153 (2018).

[15]H. Weng, R. Yu, X. Hu, X. Dai, and Z. Fang, Adv. Phys. **64**, 227 (2015).

[16]J. Zhang, B. Zhao, T. Zhou, and Z. Yang, Chin. Phys. B **25**, 117308 (2016).

[17]Y. Deng, Y. Yu, M. Z. Shi, Z. Guo, Z. Xu, J. Wang, X. H. Chen, and Y. Zhang, Science **367**, 895 (2020).

[18]C.-Z. Chang, J. Zhang, X. Feng, J. Shen, Z. Zhang, M. Guo, K. Li, Y. Ou, P. Wei, L.-L. Wang, Z.-Q. Ji, Y. Feng, S. Ji, X. Chen, J. Jia, X. Dai, Z. Fang, S.-C. Zhang, K. He, Y. Wang, L. Lu, X.-C. Ma, and Q.-K. Xue, Science **340**, 167 (2013).

[19]F. Zheng, C. Cai, S. Ge, X. Zhang, X. Liu, H. Lu, Y. Zhang, J. Qiu, T. Taniguchi, K. Watanabe, S. Jia, J. Qi, J.-H. Chen, D. Sun, and J. Feng, Adv. Mater. **28**, 4845 (2016).

[20]S. Wu, V. Fatemi, Q. D. Gibson, K. Watanabe, T. Taniguchi, R. J. Cava, and P. Jarillo-Herrero, Science

359, 76 (2018).

[21]Q. Sun, and N. Kioussis, Nanoscale **11**, 6101 (2019).

[22]Q. Sun, and N. Kioussis, Phys. Rev. B **97**, 094408 (2018).

[23]P. Li, Phys. Chem. Chem. Phys. **21**, 6712 (2019).

[24]C. Huang, J. Zhou, H. Wu, K. Deng, P. Jena, and E. Kan, Phys. Rev. B **95**, 045113 (2017).

[25]J. He, X. Li, P. Lyu, and P. Nachtigall, Nanoscale **9**, 2246 (2017).

[26]X.-L. Sheng, and B. K. Nikolić, Phys. Rev. B **95**, 201402(R) (2017).

[27]Y.-p. Wang, S.-s. Li, C.-w. Zhang, S.-f. Zhang, W.-x. Ji, P. Li, and P.-j. Wang, J. Mater. Chem. C **6**, 10284 (2018).

[28]J. Sun, X. Zhong, W. Cui, J. Shi, J. Hao, M. Xu, and Y. Li, Phys. Chem. Chem. Phys. **22**, 2429 (2020).

[29]Y. Li, Y. Liu, C. Wang, J. Wang, Y. Xu, and W. Duan, Phys. Rev. B **98**, 201407(R) (2018).

[30]G. Kresse, and J. Hafner, Phys. Rev. B **48**, 13115 (1993).

[31]G. Kresse, and J. Furthmüller, Phys. Rev. B **54**, 11169 (1996).

[32]G. Kresse, and D. Joubert, Phys. Rev. B **59**, 1758 (1999).

[33]J. P. Perdew, K. Burke, and M. Ernzerhof, Phys. Rev. Lett. **77**, 3865 (1996).

[34]A. Togo, and I. Tanaka, Scripta Mater. **108**, 1 (2015).

[35]Y. Yu, F. Yang, X. F. Lu, Y. J. Yan, Y. H. Cho, L. Ma, X. Niu, S. Kim, Y. W. Son, D. Feng, S. Li, S. W. Cheong, X. H. Chen, and Y. Zhang, Nature Nanotech. **10**, 270 (2015).

[36]K. Sugawara, Y. Nakata, R. Shimizu, P. Han, T. Hitosugi, T. Sato, and T. Takahashi, ACS Nano **10**, 1341 (2016).

[37]X. Li, Z. Zhang, and H. Zhang, Nanoscale Adv. **2**, 495 (2020).

[38]S. Zhang, J. Zhou, Q. Wang, X. Chen, Y. Kawazoe, and P. Jena, PNAS **112**, 2372 (2015).

[39]X. Chen, D. Wang, X. Liu, L. Li, and B. Sanyal, J. Phys. Chem. Lett. **11**, 2925 (2020).

[40]J. Kang, H. Sahin, and F. M. Peeters, Phys. Chem. Chem. Phys. **17**, 27742 (2015).

[41]Y. Liang, Y. Ma, P. Zhao, H. Wang, B. Huang, and Y. Dai, Appl. Phys. Lett. **116**, 162402 (2020).

[42]S. Lin, W. Li, S. Li, X. Zhang, Z. Chen, Y. Xu, Y. Chen, and Y. Pei, Joule **1**, 816 (2017).

[43]Z. Gao, F. Tao, and J. Ren, Nanoscale **10**, 12997 (2018).

[44]A. Bondi, J. Phys. Chem. **68**, 441 (1964).

[45]W. Li, N. Mingo, L. Lindsay, D. A. Broido, D. A. Stewart, and N. A. Katcho, Phys. Rev. B **85**, 195436 (2012).

[46]W. Li, J. Carrete, N. A. Katcho, and N. Mingo, Comput. Phys. Commun. **185**, 1747 (2014).

[47]W. Li, L. Lindsay, D. A. Broido, D. A. Stewart, and N. Mingo, Phys. Rev. B **86**, 174307 (2012).

[48]R. Yan, J. R. Simpson, S. Bertolazzi, J. Brivio, M. Watson, X. Wu, A. Kis, T. Luo, A. R. Hight Walker, and H. G. Xing, ACS Nano **8**, 986 (2014).

[49]B. Peng, H. Zhang, H. Shao, Y. Xu, X. Zhang, and H. Zhu, Sci. Rep. **6**, 20225 (2016).

[50]P. Zhao, Y. Ma, C. Lei, H. Wang, B. Huang, and Y. Dai, Appl. Phys. Lett. **115**, 261605 (2019).

[51]T. Abdul-Redah, P. Georgiev, D. K. Ross, M. Krzystyniak, and C. A. Chatzidimitriou-Dreismann, J. Alloy. Compd. **404–406**, 787 (2005).

[52]X. Jiang, Q. Liu, J. Xing, and J. Zhao, J. Phys. Chem. Lett. **10**, 7753 (2019).

[53]H. Zhang, Y. Ning, W. Yang, R. Zhang, and X. Xu, Nanoscale **11,** 13807 (2019).

[54]J. Heyd, G. E. Scuseria, and M. Ernzerhof, J. Chem. Phys. **118**, 8207 (2003).

[55]J. Heyd, G. E. Scuseria, and M. Ernzerhof, J. Chem. Phys. **124**, 219906 (2006).

[56]X. L. Wang, Phys. Rev. Lett. **100**, 156404 (2008).

[57]X.-L. Wang, Natl. Sci. Rev. **4**, 252 (2017).

[58]X. Wang, T. Li, Z. Cheng, X.-L. Wang, and H. Chen, Appl. Phys. Rev. **5**, 041103 (2018).

[59]Z. Yue, Z. Li, L. Sang, and X. Wang, Small **16**, 1905155 (2020).

[60]X. Wang, Z. Cheng, G. Zhang, H. Yuan, H. Chen, X.-L. Wang, Phys. Rep. DOI: https://doi.org/10.1016/j.physrep.2020.08.004 (2020).

[61]A. A. Mostofi, J. R. Yates, G. Pizzi, Y.-S. Lee, I. Souza, D. Vanderbilt, and N. Marzari, Comput. Phys. Commun. **185**, 2309 (2014).

[62]Q. S. Wu, S. N. Zhang, H.-F. Song, M. Troyer, and A. A. Soluyanov, Comput. Phys. Commun. **224**, 405 (2018).

[63]M. P. López Sancho, J. M. López Sancho, and J. Rubio, J. Phys. F: Met. Phys. **15**, 851 (1985).

[64]J. Ge, Y. Liu, J. Li, H. Li, T. Luo, Y. Wu, Y. Xu, and J. Wang, Natl. Sci. Rev. **7**, 1280 (2020).

[65]M. Nadeem, and X. Wang, arXiv:1907.07756 (2019).

[66]W.-x. Zhang, Y. Li, H. Jin, and Y.-c. She, Phys. Chem. Chem. Phys. **21**, 17740 (2019).

[67]Q. Sun, Y. Ma, and N. Kioussis, Mater. Horiz. **7**, 2071 (2020).

[68]P. Chen, J.-Y. Zou, and B.-G. Liu, Phys. Chem. Chem. Phys. **19**, 13432 (2017).

[69]K. Wang, Y. Zhang, W. Zhao, P. Li, J.-W. Ding, G.-F. Xie, and Z.-X. Guo, Phys. Chem. Chem. Phys. **21**, 9310 (2019).

PLEASE CITE THIS ARTICLE AS DOI: 10.1063/5.0023531

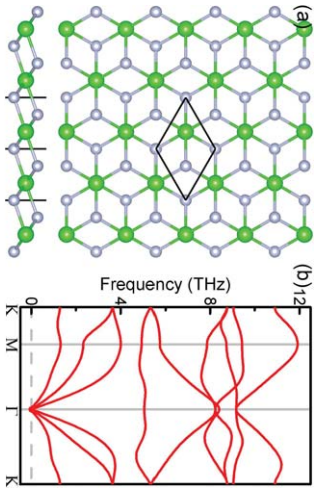

PLEASE CITE THIS ARTICLE AS DOI: 10.1063/5.0023531

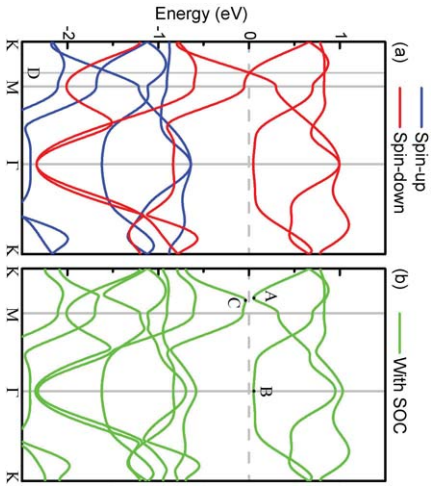

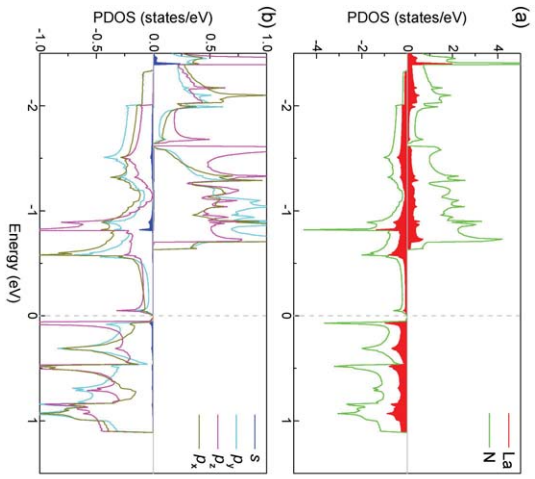

AIP Publishing

Applied Physics Letters ACCEPTED MANUSCRIPT

This is the author's peer reviewed, accepted manuscript. However, the online version of record will be different from this version once it has been copyedited and typeset.

PLEASE CITE THIS ARTICLE AS DOI: 10.1063/5.0023531